Floquet-Bloch shifts in two-band semiconductors interacting with light

Dimitrovski, Darko; Pedersen, Thomas Garm; Madsen, Lars Bojer

Published in:
Physical Review A

DOI (link to publication from Publisher):
10.1103/PhysRevA.95.063420

Publication date:
2017

Document Version
Publisher's PDF, also known as Version of record

Floquet-Bloch shifts in two-band semiconductors interacting with light

Darko Dimitrovski,[1,*] Thomas Garm Pedersen,[1] and Lars Bojer Madsen[2]
[1]*Department of Physics and Nanotechnology, Aalborg University, Skjernvej 4A 9220 Aalborg East, Denmark*
[2]*Department of Physics and Astronomy, Aarhus University, Ny Munkegade 120, 8000 Aarhus C, Denmark*
(Received 20 December 2016; published 22 June 2017)

We consider harmonic generation from a semiconductor described in the two-band approximation. In particular, the signatures of the Floquet-Bloch states in the low-order harmonic spectra are studied. We find field-strength-dependent shifts of the position of resonant peaks. The shifts are analogous to the ponderomotive shifts in strong-field physics of atoms and molecules. We illustrate this theory by analyzing low-order harmonics generated from hexagonal boron nitride.

DOI: 10.1103/PhysRevA.95.063420

I. INTRODUCTION

When the Hamiltonian for a given quantum-mechanical system is periodic in time, according to the Floquet theorem, quasienergies that form are spaced by the driving photon energy [1]. For systems periodic in space, the eigenstates are the Bloch states; see, e.g., Ref. [2]. When a strong laser field containing many cycles interacts with solids, the combination of the time and the space periodicity leads to formation of Floquet-Bloch (FB) states [3]. In that case the energy bands in solids are dressed by the laser field so that replicas of the bands appear, spaced by the photon energy. Recently, using pump-probe schemes for time- and angle-resolved photoemission spectroscopy these FB states were observed [4] and manipulated [5] on the surface of a topological insulator. Even more theoretical works have investigated the FB states. Several of them focus on graphene and the materials based on graphene—in that context the FB states were investigated for carbon nanotubes [6], for graphene in circularly polarized pulses [7], under intense THz pulses in graphene in the Dirac approximation [8] and the transition from the FB states to the Volkov states has also been considered [9].

Here we consider the signatures of the FB states in semiconductors in the two-band tight-binding approximation. We show that the FB states have a very clear signature in the harmonic responses. Specifically, we identify nonperturbative, field-strength-dependent features (peaks) in the spectra and correlate them to the appearance of the FB states. The dependency of the position of these peaks on the intensity of the pulse, but also of the peaks present in the perturbative responses, is analytically determined for a general semiconductor restricting to the features at the gap. The shifts of the peaks are analogous to the ponderomotive shifts for atoms and molecules known in strong-field physics. We verify the analysis by comparison with the full numerical calculations modeling low-order harmonic responses from hexagonal boron nitride (*h*-BN), a gapped-graphene-type [10–15] of material [15], similar to MoS_2 [16] for which high-order harmonic generation (HHG) spectra have recently been obtained experimentally [17].

The paper is organized as follows: In the next section we present the basic theory for harmonic generation from semiconductors in the two-band tight-binding approximation. In Sec. III we analyze harmonic generation from a two-band system by using the Floquet formalism, and we establish analogies with the Floquet states in a two-level atom. On the basis of these analogies and by using the effective mass approximation at the gap, we uncover the field-dependent FB shifts of the resonant peaks in the harmonic responses. In Sec. IV we proceed to verify these shifts and the appearance of novel peaks due to FB states by comparing the full calculation with the theory for the first and second harmonic of *h*-BN. The conclusions are given in the last section.

II. THEORY OF INTERACTION OF TWO-BAND SYSTEM WITH LIGHT

For a two-band system the wave function can be written as

$$\Psi(\mathbf{r},t) = \sum_{m=c,v} \int_{\mathrm{BZ}} a_m(\mathbf{k},t)\psi_{m,\mathbf{k}}(\mathbf{r})d^3\mathbf{k}, \tag{1}$$

where BZ denotes that the integration is performed over the Brillouin zone, c and v denote the conduction and valence bands, respectively, and

$$\psi_{m,\mathbf{k}}(\mathbf{r}) = u_{m\mathbf{k}}(\mathbf{r})\exp(i\mathbf{k}\cdot\mathbf{r}) \tag{2}$$

are the Bloch wave functions—eigenfunctions of the field-free Hamiltonian $\hat{H}_0$, i.e., $\hat{H}_0\psi_{m,\mathbf{k}} = E_m(\mathbf{k})\psi_{m,\mathbf{k}}(\mathbf{r})$.

Without loss of generality, for the moment we assume that the two-band system possesses a gap Δ (Fig. 1), and that in the vicinity of the gap the energy dispersion can be described by using the effective mass approximation, i.e., by approximating the energies of the valence and the conduction band as

$$E_c(\mathbf{k}) = E_{c0} + \frac{\hbar^2k^2}{2m_e^*}, \quad E_v(\mathbf{k}) = E_{v0} - \frac{\hbar^2k^2}{2m_h^*}; \tag{3}$$

see Fig. 1. In the above equation, E_{c0} and E_{v0} are the energies of the conduction and the valence bands at the gap point $\Delta = E_{c0} - E_{v0}$, and m_e^* and m_h^* are the effective masses of the electron and hole, respectively.

When interacting with light, in the length gauge, the Hamiltonian reads $\hat{H}(t) = \hat{H}_0 + e\mathbf{F}(t)\cdot\mathbf{r}$, where $\mathbf{F}(t)$ is the electric field of the laser and e is the norm of the electron charge. The a_m from Eq. (1) satisfy the following equations of motion [18]:

$$\dot{a}_m = \left(-\frac{i}{\hbar}E_m(\mathbf{k}) + \frac{e}{\hbar}\mathbf{F}(t)\cdot\nabla_{\mathbf{k}}\right)a_m - i\frac{e}{\hbar}\mathbf{F}(t)\cdot\sum_n \boldsymbol{\xi}_{mn}(\mathbf{k})a_n, \tag{4}$$

*dd@nano.aau.dk

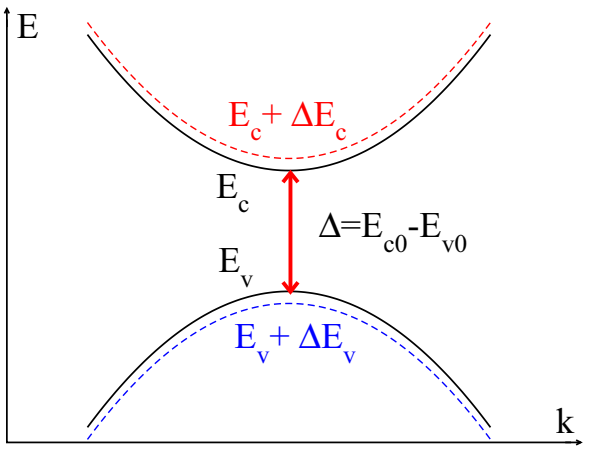

FIG. 1. Sketch of the band structure. The energies of the conduction band (E_c), the valence band (E_v), and the band gap Δ are illustrated. The dashed lines depict the valence and the conduction bands in strong fields, revealing the Floquet-Bloch shifts.

where

$$\boldsymbol{\xi}_{mn}(\mathbf{k}) = i\int u^*_{m\mathbf{k}}(\mathbf{r})\nabla_{\mathbf{k}}u_{n\mathbf{k}}(\mathbf{r})d^3\mathbf{r}, \tag{5}$$

$n,m \in (c,v)$, and where the dependence of a_m and a_n on $\mathbf{k}$ and t is omitted to ease notation. The explicit expressions for the $\boldsymbol{\xi}$ of Eq. (5) depend on the system in question. For a gapped graphene, explicit expressions can be found in, e.g., Ref. [19].

The amplitude equations (4) do not readily allow inclusion of decoherence and temperature effects. For this purpose, the equations of motion can be reformulated by using the density matrix

$$\rho = \begin{pmatrix}\rho_{cc} & \rho_{cv}\\ \rho_{vc} & \rho_{vv}\end{pmatrix} = \begin{pmatrix}|a_c|^2 & a_c a_v^*\\ a_v a_c^* & |a_v|^2\end{pmatrix}. \tag{6}$$

We rewrite the system of equations (4) following Ref. [18] and by adding a term containing the decoherence time τ to introduce a decay, we obtain the following coupled equations of motion (see Ref. [19] for details):

$$\begin{aligned}\frac{d\rho_{cv}(\mathbf{k},t)}{dt} &= -i\frac{E_{cv}(\mathbf{k})}{\hbar}\rho_{cv}(\mathbf{k},t) - i\frac{e}{\hbar}\mathbf{F}(t)\cdot\boldsymbol{\xi}_{cv}(\mathbf{k})n(\mathbf{k},t)\\ &+ \frac{e}{\hbar}\mathbf{F}(t)\cdot\nabla_{\mathbf{k}}\rho_{cv}(\mathbf{k},t)\\ &- i\frac{e}{\hbar}\mathbf{F}(t)\cdot[\boldsymbol{\xi}_{cc}(\mathbf{k})-\boldsymbol{\xi}_{vv}(\mathbf{k})]\rho_{cv}(\mathbf{k},t) - \frac{\rho_{cv}(\mathbf{k},t)}{\tau},\end{aligned} \tag{7}$$

$$\begin{aligned}\frac{dn(\mathbf{k},t)}{dt} &= 2i\frac{e}{\hbar}\mathbf{F}(t)\cdot[\boldsymbol{\xi}_{cv}(\mathbf{k})\rho^*_{cv}(\mathbf{k},t) - \boldsymbol{\xi}^*_{cv}(\mathbf{k})\rho_{cv}(\mathbf{k},t)]\\ &+ \frac{e}{\hbar}\mathbf{F}(t)\cdot\nabla_{\mathbf{k}}n(\mathbf{k},t) - \frac{n(\mathbf{k},t)-[f_v(\mathbf{k},T)-f_c(\mathbf{k},T)]}{\tau},\end{aligned} \tag{8}$$

where $n = \rho_{vv} - \rho_{cc}$, $E_{cv}(\mathbf{k}) = E_c(\mathbf{k}) - E_v(\mathbf{k})$, and

$$f_m(\mathbf{k},T) = \left[1+\exp\left(\frac{E_m(\mathbf{k})}{k_BT}\right)\right]^{-1} \tag{9}$$

is the Fermi-Dirac distribution for the conduction and valence band, respectively. In the above equation, $m = c,v$ denotes the conduction and the valence band, respectively, k_B is Boltzmann's constant, and T is the temperature. Note that, to obtain Eqs. (7) and (8), we did not invoke the effective mass approximation. The equations of motion for a particular system, (7) and (8), are solved with the initial conditions $\rho_{cv}(\mathbf{k},-\infty) = 0$ and $n(\mathbf{k},-\infty) = f_v(\mathbf{k},T) - f_c(\mathbf{k},T)$.

The current is given by $\mathbf{J}(t) = -2\frac{e}{m_e}\mathrm{Tr}\{\hat{\mathbf{p}}\rho\}$ [18], where the factor of two stands for the spin multiplicity. Explicitly, the current is calculated as [18,19]

$$\begin{aligned}\mathbf{J}(t) = -\frac{e}{\pi^2 m_e}\Bigg[&\int d\mathbf{k}[\mathbf{p}_{vc}(\mathbf{k})\rho_{cv}(\mathbf{k},t) + \mathbf{p}_{cv}(\mathbf{k})\rho_{vc}(\mathbf{k},t)]\\ &+ \int d\mathbf{k}\frac{1}{2}[\mathbf{p}_{vv}(\mathbf{k}) - \mathbf{p}_{cc}(\mathbf{k})]n(\mathbf{k},t)\Bigg].\end{aligned} \tag{10}$$

The form of the momentum matrix elements $p_{nm}(\mathbf{k})$, $m,n \in (c,v)$, will be discussed in Sec. IV. The first integral in Eq. (10) is the interband current, while the second integral is the intraband current. The harmonic spectrum is obtained as the Fourier transform of the current: $\mathbf{j}(\Omega) = \mathcal{F}\{\mathbf{J}(t)\}$. In Sec. IV we consider numerical harmonic spectra based on the formalism of this section.

III. FLOQUET ANALYSIS OF INTERACTION OF TWO-BAND SYSTEM WITH LASER LIGHT

A. Transformation of equations of motion

To make a connection between the laser-semiconductor interaction and the laser-atom interaction, it is beneficial to transform the amplitude equations of motion (4) into the Houston basis [20,21]. Following [20–22], we introduce the transformation

$$a_m(\mathbf{k},t) = c_m(\mathbf{K},t)e^{-\frac{i}{\hbar}\int^t\{E_m(\mathbf{k},t')+e\mathbf{F}(t')\cdot\boldsymbol{\xi}_{mm}[\mathbf{K}+\frac{e}{\hbar}\mathbf{A}(t')]\}dt'}, \tag{11}$$

where $m \in (c,v)$. In the above equation, we introduced the shifted wave vector

$$\mathbf{K} = \mathbf{k} - \frac{e}{\hbar}\mathbf{A}(t), \tag{12}$$

where $\mathbf{A}(t) = -\int^t dt'\mathbf{F}(t')$ is the vector potential and $e\mathbf{A}(t)$ is the momentum gain of a free electron in the field. Using the above transform, Eqs. (4) become

$$\begin{aligned}i\hbar\frac{dc_c(\mathbf{K},t)}{dt} &= e\mathbf{F}(t)\cdot\boldsymbol{\xi}_{cv}\left(\mathbf{K}+\frac{e}{\hbar}\mathbf{A}(t)\right)c_v(\mathbf{K},t)\\ &\times e^{i[S(\mathbf{K},t)+W(\mathbf{K},t)]},\\ i\hbar\frac{dc_v(\mathbf{K},t)}{dt} &= e\mathbf{F}(t)\cdot\boldsymbol{\xi}^*_{cv}\left(\mathbf{K}+\frac{e}{\hbar}\mathbf{A}(t)\right)c_c(\mathbf{K},t)\\ &\times e^{-i[S(\mathbf{K},t)+W(\mathbf{K},t)]},\end{aligned} \tag{13}$$

where the phases are given by

$$S(\mathbf{K},t) = \frac{1}{\hbar}\int^t E_{cv}\left(\mathbf{K}+\frac{e}{\hbar}\mathbf{A}(t')\right)dt', \tag{14}$$

$$\begin{aligned}W(\mathbf{K},t) = \frac{e}{\hbar}\int^t\mathbf{F}(t')\cdot\Bigg[&\boldsymbol{\xi}_{cc}\left(\mathbf{K}+\frac{e}{\hbar}\mathbf{A}(t')\right)\\ &-\boldsymbol{\xi}_{vv}\left(\mathbf{K}+\frac{e}{\hbar}\mathbf{A}(t')\right)\Bigg]dt'.\end{aligned} \tag{15}$$

The equations (13) are mathematically identical to the equations of motion (4) from where the density matrix equations (7) and (8), which are used to obtain the harmonic spectra, are constructed. We note that the term $\nabla_{\mathbf{k}}$, present in Eq. (4), is absorbed through the introduction of the shifted wave vector $\mathbf{K}$ of Eq. (12) as an argument in Eq. (13). Without such a term, field-dependent phases [Eqs. (14) and (15)] would not appear.

B. Analogy with two-level system

For a few-level atom interacting with light, HHG spectra have been analyzed by using the Floquet formalism [23–26]. Here, we exploit the similarity between the system described by Eq. (13) at fixed $\mathbf{K}$ and the equation for a two-level system (two-level approximation of an atomic system), formally used to analyze eigenenergies of a Floquet Hamiltonian [1]. More precisely, for a two-level system interacting with an infinitely periodic laser field, the equations of motions for the amplitudes C_c and C_v of the "upper" and "lower" state with eigenenergies E_c and E_v, respectively, are

$$\begin{aligned} i\hbar\frac{dC_c(t)}{dt} &= D\cos(\omega t)e^{\frac{i}{\hbar}(E_c-E_v)t}C_v(t),\\ i\hbar\frac{dC_v(t)}{dt} &= D^*\cos(\omega t)e^{-\frac{i}{\hbar}(E_c-E_v)t}C_c(t), \end{aligned} \tag{16}$$

where D is the product of the dipole matrix element between the states and the field amplitude F_0, while $\cos(\omega t)$ stems from the field time dependence. In this way the Hamiltonian of this system is periodic in time, and the above system of differential equations can be solved by application of the Floquet theorem. It emerges [1] that the eigenenergies of such a system are obtained by diagonalization of the following matrix with infinite dimensions:

$$\begin{pmatrix} \cdot & \cdot & \cdot & \cdot & \cdot & \cdot & \cdot & \cdot \\ \cdot & E_c-\hbar\omega & 0 & 0 & D/2 & 0 & 0 & \cdot \\ \cdot & 0 & E_v-\hbar\omega & D^*/2 & 0 & 0 & 0 & \cdot \\ \cdot & 0 & D/2 & E_c & 0 & 0 & D/2 & \cdot \\ \cdot & D^*/2 & 0 & 0 & E_v & D^*/2 & 0 & \cdot \\ \cdot & 0 & 0 & 0 & D/2 & E_c+\hbar\omega & 0 & \cdot \\ \cdot & 0 & 0 & D^*/2 & 0 & 0 & E_v+\hbar\omega & \cdot \\ \cdot & \cdot & \cdot & \cdot & \cdot & \cdot & \cdot & \cdot \end{pmatrix}. \tag{17}$$

For small off-diagonal matrix elements D, the eigenenergies of the above matrix, or in other terms, the Floquet state energies, are approximately

$$E_m \pm j\hbar\omega, \tag{18}$$

with $m = c, v$ denoting the bands and $j = 0,1,2,\ldots$ the number of photons. The above does not apply at the points where the eigenenergies of Eq. (17) exhibit avoided crossings as a function of the peak field strength, then explicit diagonalization is needed. We label the obtained Floquet states by the pair (m, j).

The interaction of the strong laser field with solids creates FB states—the valence and the conduction bands are dressed by the photon field [3]. As stated in the Introduction, these states were detected experimentally by using an elaborate pump-probe scheme [4,5]. Here we show, by using the analogy with the two-level system, that the FB states have a very clear signature in the harmonic spectra produced by a single laser pulse.

The system of equations (13) can be analyzed by using the methods used in the case of the two-level system (16). The difference is that, to obtain any laser-induced response for a solid—a measurable current or harmonic response—it has to be integrated over $\mathbf{K}$. In the analysis, we assume that exactly at $\mathbf{K}$ corresponding to the gap between the valence and conduction band, the dipole matrix elements are maximized and a resonance appears in the harmonic spectra at these photon energies. Therefore, the dynamics at this point dominates the harmonic response. Similarly to Refs. [27,28], we limit the analysis to this point, however, in Sec. IV we compare it with the full numerical solution. Finally, although we will use the Floquet approach to analyze the peaks in the harmonic spectra, we will not use it to solve the dynamics as we obtain the solution numerically on the grid using Eqs. (7) and (8).

C. Floquet-Bloch shifts

The energy phases are crucial in establishing the analogy between the two-level system [Eq. (16)] and the semiconductor [Eq. (13)]. There is, of course, a difference between the energy phases in Eqs. (13) and (16); that is, between

$$\frac{1}{\hbar}(E_c - E_v)t, \tag{19}$$

which is linear in t and independent of the peak field strength F_0, and the field-dependent phase

$$S(\mathbf{K},t) + W(\mathbf{K},t). \tag{20}$$

We exploit the formal similarity between Eqs. (16) and (13) in the sense that the phase (20) in Eq. (13) plays the role of the phase (19) in Eq. (16). Then, to compare directly with the case of the two-level system, by using Floquet analysis we proceed to replace the integrand in the phase of Eq. (20) with its time average $\langle . \rangle_t = (1/T_p)\int_0^{T_p} dt(.)$, $T_p = 2\pi/\omega$, i.e.,

$$\begin{aligned} &\frac{1}{\hbar}\left\langle E_c\left(\mathbf{K}+\frac{e}{\hbar}\mathbf{A}(t)\right)\right\rangle_t - \frac{1}{\hbar}\left\langle E_v\left(\mathbf{K}+\frac{e}{\hbar}\mathbf{A}(t)\right)\right\rangle_t \\ &\quad + \frac{e}{\hbar}\left\langle \mathbf{F}(t)\cdot\left[\boldsymbol{\xi}_{cc}\left(\mathbf{K}+\frac{e}{\hbar}\mathbf{A}(t)\right) - \boldsymbol{\xi}_{vv}\left(\mathbf{K}+\frac{e}{\hbar}\mathbf{A}(t)\right)\right]\right\rangle_t, \end{aligned} \tag{21}$$

where we have used the definitions in Eqs. (14) and (15). From the analysis below it will be evident that this time-averaged phase enters the Floquet matrix in the diagonal matrix elements, just as the energies E_v and E_c enter Eq. (17) for the two-level system.

Next, we expand the phase of Eq. (21) in orders of field strength and retain the first nonzero field-dependent term. The last term in Eq. (21) vanishes in any order of field strength since $\int_0^{T_p} dt \sin(\omega t)\cos^n(\omega t) = 0$ and, equally, $\int_0^{T_p} dt \cos(\omega t)\sin^n(\omega t) = 0$. The time average of the terms contained in the first line in Eq. (21) is nonzero. Expanding in first nonzero order of the peak field strength F_0, we obtain

$$\left\langle E_{c/v}\left(\mathbf{K}+\frac{e}{\hbar}\mathbf{A}(t)\right)\right\rangle_t \approx E_{c/v}(\mathbf{K}) + \Delta E_{c/v}, \tag{22}$$

where

$$\Delta E_{c/v} = \frac{1}{2}\frac{d^2E_{c/v}}{dK_{\mathbf{F}}^2}\frac{e^2}{\hbar^2}\langle A^2(t)\rangle_t, \tag{23}$$

and where $K_{\mathbf{F}} = \mathbf{K}\cdot\mathbf{e}_{\mathbf{F}}$ is the component of $\mathbf{K}$ along the field direction $\mathbf{e}_{\mathbf{F}}$.

As stated above, we limit the analysis to the $\mathbf{K}$ corresponding to the gap, so $E_c(\mathbf{K}) = E_{c0}$ and $E_v(\mathbf{K}) = E_{v0}$. At the gap we assume the effective mass approximation [Eq. (3)], therefore the direction in the derivative (23) does not matter so $d^2E_c/dK_{\mathbf{F}}^2 = \hbar^2/m_e^*$ and $d^2E_v/dK_{\mathbf{F}}^2 = -\hbar^2/m_h^*$. Hence the first nonvanishing field dependent terms give the following shifts of the energy bands by the strong laser field:

$$\Delta E_c = \frac{e^2}{4m_e^*}\frac{F_0^2}{\omega^2} \text{ and } \Delta E_v = -\frac{e^2}{4m_h^*}\frac{F_0^2}{\omega^2}. \tag{24}$$

These shifts are illustrated as differences between the full and the dashed curves in Fig. 1. Note that, although from the sketch of the energy bands in Fig. 1 it might look as if for each $\mathbf{k}$ the shift is the same, this is not true. In the following we are interested in the shift corresponding to the gap. We note that the shifts are most likely present at other $\mathbf{K}$ points where the dipole matrix element does not peak; however, they do not produce any visible resonance in the harmonic spectrum and therefore such shifting cannot be observed.

We denote the total shift of the valence and the conduction band at the gap as the Floquet-Bloch (FB) shift. The explicit expression for the FB shift hence reads

$$E^{FB}(F_0,\omega) = \frac{e^2}{4\mu}\frac{F_0^2}{\omega^2}, \tag{25}$$

where $\mu^{-1} = m_e^{*-1} + m_h^{*-1}$ is the reduced effective mass. Because of the shifts in the valence and the conduction band [Eq. (24)], the Floquet matrix for the system (13) at K corresponding to the gap contains diagonal matrix elements that are shifted with respect to the diagonal matrix elements for atoms (17), i.e., E_c is replaced by

$$E_c^{(1)} = E_c + \Delta E_c, \tag{26}$$

and E_v is replaced by

$$E_v^{(1)} = E_v + \Delta E_v. \tag{27}$$

As in the case of the two-level system [Eq. (16)] we label the FB states by the pair (m,j). The approximate eigenenergies of the FB states [Eqs. (26) and (27)] are shifted with respect to the Floquet energies (18) of the two-level system.

Next, for systems for which the Floquet states are defined by the matrix of Eq. (17), the coupling between different states is through an odd number of photons. Hence states (c,j) and $(v,j\pm 2q)$, where q is a positive integer, do not couple and belong to orthogonal spaces, effectively forbidding two-photon transitions between c and v states. For excited atoms and systems for which inversion symmetry with respect to the plane perpendicular to the field is broken there are couplings that lead to the appearance of even-photon resonances. Specializing to the FB states, and considering Eq. (13), two-photon transitions are enabled from the explicit time dependence of the energy phase of Eq. (20) and of the dipole matrix element $\boldsymbol{\xi}_{cv}$ [Eq. (13)]. Assuming an infinite periodic field, in first nonvanishing order of field strength the phase reads

$$W(\mathbf{K},t) \approx \frac{e}{\hbar}\frac{F_0}{\omega}\{[\boldsymbol{\xi}_{cc}(\mathbf{K}) - \boldsymbol{\xi}_{vv}(\mathbf{K})]\cdot\mathbf{e}_{\mathbf{F}}\}\sin(\omega t). \tag{28}$$

This term, which is of first order in field strength, indirectly enables two-photon coupling between the valence- and conduction-band Floquet energies. To see that, we rewrite Eq. (13), eliminating W in the phase by the transformation

$$b_m(\mathbf{K},t) = c_m(\mathbf{K},t)e^{-\frac{i}{\hbar}\int^t\{e\mathbf{F}(t')\cdot\boldsymbol{\xi}_{mm}[\mathbf{K}+\frac{e}{\hbar}\mathbf{A}(t')]\}dt'}, \tag{29}$$

such that Eq. (13) becomes

$$\begin{aligned}
i\hbar\frac{db_c(\mathbf{K},t)}{dt} &= e\mathbf{F}(t)\cdot\boldsymbol{\xi}_{cv}\left(\mathbf{K}+\frac{e}{\hbar}\mathbf{A}(t)\right)b_v(\mathbf{K},t)e^{iS(\mathbf{K},t)} \\
&\quad + e\mathbf{F}(t)\cdot\boldsymbol{\xi}_{cc}\left(\mathbf{K}+\frac{e}{\hbar}\mathbf{A}(t)\right)b_c(\mathbf{K},t), \\
i\hbar\frac{db_v(\mathbf{K},t)}{dt} &= e\mathbf{F}(t)\cdot\boldsymbol{\xi}_{cv}^*\left(\mathbf{K}+\frac{e}{\hbar}\mathbf{A}(t)\right)b_c(\mathbf{K},t)e^{-iS(\mathbf{K},t)} \\
&\quad + e\mathbf{F}(t)\cdot\boldsymbol{\xi}_{vv}\left(\mathbf{K}+\frac{e}{\hbar}\mathbf{A}(t)\right)b_v(\mathbf{K},t).
\end{aligned} \tag{30}$$

The diagonal terms in the system of equations (30) enable one-photon coupling to the Floquet states within the conduction and the valence band, separately. In the first nonvanishing order of the field strength,

$$\begin{aligned}
e\mathbf{F}(t)\cdot\boldsymbol{\xi}_{cc}\left(\mathbf{K}+\frac{e}{\hbar}\mathbf{A}(t)\right) &\approx eF_0[\boldsymbol{\xi}_{cc}(\mathbf{K})\cdot\mathbf{e}_{\mathbf{F}}]\cos(\omega t) \\
&= D_{cc}\cos(\omega t),
\end{aligned} \tag{31}$$

$$\begin{aligned}
e\mathbf{F}(t)\cdot\boldsymbol{\xi}_{vv}\left(\mathbf{K}+\frac{e}{\hbar}\mathbf{A}(t)\right) &\approx eF_0[\boldsymbol{\xi}_{vv}(\mathbf{K})\cdot\mathbf{e}_{\mathbf{F}}]\cos(\omega t) \\
&= D_{vv}\cos(\omega t).
\end{aligned} \tag{32}$$

The term $D_{cc}\cos(\omega t)$ couples the states $(c,j\pm 1)$ and (c,j), while $D_{vv}\cos(\omega t)$ couples the states (v,j) and $(v,j\pm 1)$. With this coupling, an indirect two-photon coupling between the states (c,j) and $(v,j\pm 2q)$ is enabled. We note that both D_{cc} and D_{vv} are of first order in field strength.

Since the dipole transition matrix elements $\boldsymbol{\xi}_{cv}[\mathbf{K}+(e/\hbar)\mathbf{A}(t)]$ of Eq. (13) are field dependent, in principle, all photon orders of coupling are present. Up to the second order

in field strength,

$$\begin{aligned} & e\mathbf{F}(t)\cdot\boldsymbol{\xi}_{cv}\Big(\mathbf{K}+\frac{e}{\hbar}\mathbf{A}(t)\Big) \\ & \approx eF_0[\boldsymbol{\xi}_{cv}(\mathbf{K})\cdot\mathbf{e}_\mathbf{F}]\cos(\omega t) \\ & \quad -\frac{e^2F_0^2}{2\hbar\omega}\{\mathbf{e}_\mathbf{F}\cdot\boldsymbol{\nabla}_\mathbf{k}[\boldsymbol{\xi}_{cv}(\mathbf{K})\cdot\mathbf{e}_\mathbf{F}]\}\sin(2\omega t) \\ & = D\cos(\omega t)+\Delta D\sin(2\omega t). \end{aligned} \tag{33}$$

The term $D\cos(\omega t)$ couples the states $(c, j\pm 1)$ and (v, j). This term, which is of first order in field strength, is present for atoms as well; see the Floquet matrix of Eq. (17). The term $\Delta D\sin(2\omega t)$, which is of second order in field strength, couples the states $(c, j\pm 2)$ and (v, j), and therefore directly enables two-photon transitions between the valence and conduction bands.

To construct the Floquet matrix for FB states we include (i) the energy shifts $\Delta E_{c/v}$ [Eqs. (26) and (27)] of second order in field strength in the diagonal matrix elements, (ii) the one-photon coupling within the conduction band D_{cc} [Eq. (31)] and within the valence band D_{vv} [Eq. (32)], and (iii) the first nonzero correction to the transition dipole element in the off-diagonal terms of the matrix ΔD [Eq. (33)] that induces a coupling between the valence and conduction band. With these ingredients, the following matrix defines the FB states in semiconductors,

$$\begin{pmatrix} \cdot & \cdot & \cdot & \cdot & \cdot & \cdot & \cdot & \cdot \\ \cdot & E_c+\Delta E_c-\hbar\omega & 0 & D_{cc}/2 & D/2 & 0 & i\Delta D/2 & \cdot \\ \cdot & 0 & E_v+\Delta E_v-\hbar\omega & D^*/2 & D_{vv}/2 & i\Delta D^*/2 & 0 & \cdot \\ \cdot & D_{cc}/2 & D/2 & E_c+\Delta E_c & 0 & D_{cc}/2 & D/2 & \cdot \\ \cdot & D^*/2 & D_{vv}/2 & 0 & E_v+\Delta E_v & D^*/2 & D_{vv}/2 & \cdot \\ \cdot & 0 & -i\Delta D/2 & D_{cc}/2 & D/2 & E_c+\Delta E_c+\hbar\omega & 0 & \cdot \\ \cdot & -i\Delta D^*/2 & 0 & D^*/2 & D_{vv}/2 & 0 & E_v+\Delta E_v+\hbar\omega & \cdot \\ \cdot & \cdot & \cdot & \cdot & \cdot & \cdot & \cdot & \cdot \end{pmatrix}. \tag{34}$$

Due to the off-diagonal, field-dependent terms D in the Floquet matrix (17), the Bloch-Siegert shifts [29] appear as well. In the perturbative limit and close to a particular resonance between the Floquet states, an analytic expression can be derived as follows (see Ref. [1]): We assume that $\hbar\omega$ is almost resonant with the transition between, say, (c, j) and $(v, j+1)$. Then in the perturbative limit the interaction from the states $(v, j-1)$ and $(c, j+2)$ can be incorporated and the perturbative matrix [1] reads

$$\begin{pmatrix} E_c+j\hbar\omega+\frac{|D|^2}{8\hbar\omega} & D/2 \\ D^*/2 & E_v+(j+1)\hbar\omega-\frac{|D|^2}{8\hbar\omega}-\hbar\omega \end{pmatrix}, \tag{35}$$

from where the correction terms involving $|D|^2$ appear. These are obtained by approximating E_c-E_v with $\hbar\omega$. Then due to the action of this correction term, the Bloch-Siegert shift $|D|^2/(4\hbar\omega)$ appears, and the resonance frequency ω_R is to be found from

$$\hbar\omega_R = E_c-E_v+\frac{|D|^2}{4\hbar\omega_R}. \tag{36}$$

The same consideration applies for the semiconductor case by replacing E_c and E_v with $E_c^{(1)}$ and $E_v^{(1)}$ of Eqs. (26) and (27), respectively. The resonance frequency for the transition at the gap $\Delta = E_{c0}-E_{v0}$, using shifts to second order in field strength, reads

$$\hbar\omega_R = \Delta + E^{FB}(F_0,\omega_R)+\frac{e^2F_0^2|\boldsymbol{\xi}_{cv}\cdot\mathbf{e}_{\mathbf{F}_0}|^2}{4\hbar\omega_R}, \tag{37}$$

where $\boldsymbol{\xi}_{cv}$ is evaluated at the gap.

For the case of two-photon transitions between the FB states at the gap, the resonance frequencies, using energy shifts to second order in field strength, are equal to

$$2\hbar\omega_R = \Delta + E^{FB}(F_0,\omega_R). \tag{38}$$

Note that in the next nonzero order of the field strength, the fourth order of field strength, a term analogous to the Bloch-Siegert shift in Eq. (37) should appear, however here it involves ΔD rather than D.

D. Meaning of Floquet–Bloch shifts

The FB shifts of Eq. (25), appearing also in Eqs. (37) and (38), are of the same order in field strength as the Bloch-Siegert shifts. Contrary to the Bloch-Siegert shifts, for which analytic expressions are available in the perturbative limit, the FB shifts can be read directly from the diagonal matrix elements in the Floquet matrix (34) and therefore are easily analytically evaluated. Moreover, by including additional terms in the Taylor expansion of the time-averaged energy (22) it is possible to obtain corrections to higher orders in the field strength for the FB shifts.

The expression for the FB shift [Eq. (25)] is formally identical to the expression for the ponderomotive shift U_p in strong-field physics, $U_p = (eF_0)^2/(4m_e\omega^2)$, where m_e is the electron mass. Here, the FB shift emerged from the Volkov-like phase $S(\mathbf{K},t)$ [Eq. (14)] that in turn was obtained from the transformation of the equations of motions in the Houston basis. In the early paper by Keldysh [30], where the foundations of strong-field physics for atomic systems were made, strong-field laser-solid interaction was also considered. From the analysis in that paper it emerges that these shifts in solids come from the time average of the Volkov-like phase $S(\mathbf{K},t)$. Specifically, when the total rate of transfer from the valence to the conduction band is considered, the effective gap in the multiphoton regime is introduced in Eq. (42) of that paper. The reason why this effective gap appears there is because a response to an infinite periodic pulse is considered and therefore the transition amplitude was expanded in a

Fourier series, which implicitly amounts to performing Floquet analysis within the Keldysh approximation.

Hence, this FB shift can be thought of as a ponderomotive shift for valence and conduction bands in semiconductors. This interpretation and the analogy with the strong-field physics also helps to establish the limits of the validity of the perturbative response in semiconductors. Namely, the point of breakdown of the perturbation theory and the onset of the strong-field regime is the point when the ratio $U_p/(\hbar\omega)$, denoted as nonperturbative intensity parameter [31], becomes non-negligible. Analogously, for semiconductors, the breakdown of perturbation theory starts when the ratio

$$\frac{E^{FB}(F_0,\omega_R)}{\hbar\omega} = \frac{e^2}{4\hbar\mu}\frac{F_0^2}{\omega^3} \tag{39}$$

becomes non-negligible. Under the assumption that the major part of the nth-order perturbative response is located in the vicinity of the photon energies $\hbar\omega = \Delta/n$, we can deduce that the condition for the validity of perturbation theory for the nth-order response is

$$\frac{e^2F_0^2\hbar^2n^3}{4\Delta^3\mu} \ll 1. \tag{40}$$

From the above inequality we can conclude that the perturbation theory breaks down at lower field strengths for the higher-order harmonics. This has already been observed by performing explicit numerical calculations [19].

In the following, to illustrate the emergence of the signatures of the FB states in the harmonic spectra and the FB shifts, we consider harmonic generation from h-BN as a nontrivial, realistic example.

IV. EXAMPLE: HARMONIC GENERATION FROM h-BN

A band gap in graphene can be induced in several ways [10–14]. For the purpose of our analysis, we focus on h-BN, where two carbon atoms in the unit cell are replaced by a h-BN dimer [Fig. 2(a)], with $a = 2.49$ Å. To describe the interaction of the hexagonal h-BN with light we can use the model of gapped graphene [15]. For gapped graphene, similarly to graphene [32], in the basis consisting of two Bloch wave functions (for details, see Ref. [19]), the tight-binding

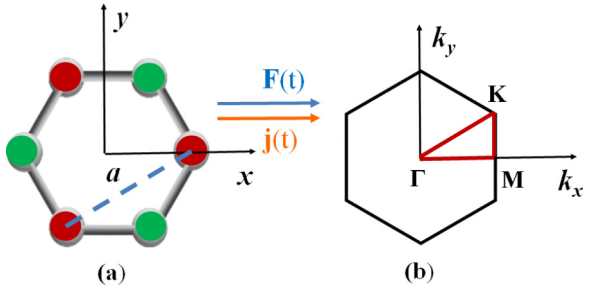

FIG. 2. (a) The structure of h-BN in position space. The different shades (colors) at the points of the hexagon denote B and N atoms, respectively. The characteristic distance $a = 2.49$ Å, as well as the orientation of the laser pulse $\mathbf{F}(t)$ and the current $\mathbf{j}(t)$ are shown. (b) Brillouin zone in reciprocal space. The Γ, M, and K points are denoted as vertices of a triangle sketched in red.

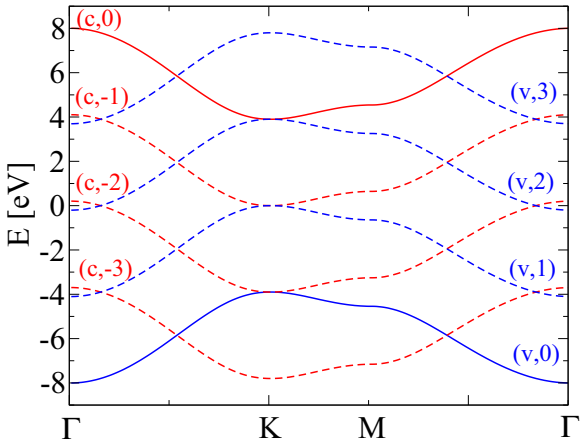

FIG. 3. Energy bands in h-BN. Full lines: field-free energy bands in h-BN. Dashed lines: approximate energies of the FB states. As an example we plot $E_c(\mathbf{k}) - j\hbar\omega$ and $E_v(\mathbf{k}) + j\hbar\omega$, $j = 1,2,3$ for $\hbar\omega = \Delta/2$. The bands are plotted along the thick (red) triangle in Fig. 2(b) in the reciprocal ($\mathbf{k}$) space connecting Γ, M, and K points.

Hamiltonian is obtained as [33]

$$\hat{\mathbf{H}}_0 = \begin{bmatrix} \frac{\Delta}{2} & -\gamma f(\mathbf{k}) \\ -\gamma f^*(\mathbf{k}) & -\frac{\Delta}{2} \end{bmatrix}, \tag{41}$$

where Δ is the energy gap, $\gamma = -\langle p_z(\mathbf{r}-\mathbf{R}_A)|\hat{H}|p_z(\mathbf{r}-\mathbf{R}_B)\rangle \approx 2.33$ eV [34] is the hopping integral, and

$$f(\mathbf{k}) = \exp\left(i\frac{ak_x}{\sqrt{3}}\right) + 2\exp\left(-i\frac{ak_x}{2\sqrt{3}}\right)\cos\left(\frac{ak_y}{2}\right) \tag{42}$$

comes from the geometry of the location of the nearest neighbors. The energies of the valence band,

$$E_v(\mathbf{k}) = -\sqrt{\left(\frac{\Delta}{2}\right)^2 + \gamma^2|f(\mathbf{k})|^2}, \tag{43}$$

and conduction band,

$$E_c(\mathbf{k}) = \sqrt{\left(\frac{\Delta}{2}\right)^2 + \gamma^2|f(\mathbf{k})|^2}, \tag{44}$$

are obtained by diagonalization of the Hamiltonian of Eq. (41). These energies are plotted as full lines in Fig. 3 along the triangle in $\mathbf{k}$ space [thick (red) triangle in Fig. 2(b)] whose vertices are the Γ, M, and K points.

To calculate the current of Eq. (10), we use the diagonal momentum matrix elements as $\mathbf{p}_{nn} = \frac{m_e}{\hbar}\frac{\partial E_n}{\partial \mathbf{k}}$, while the off-diagonal momentum matrix elements are obtained as $\mathbf{p}_{nm} = im_e\omega_{nm}\boldsymbol{\xi}_{nm}$ [18]. The explicit expressions for the momentum matrix elements can be found in, e.g., Appendix B in Ref. [19].

The numerical approach for solving of the equations of motion (7) and (8) consists of using a rectangular $\mathbf{k}$ grid (around 250 points in each dimension) and approximating the gradients with balanced difference [35]. The time propagation is performed using an adaptive Runge-Kutta algorithm. We use $T = 10$ K [Eq. (9)] and $\tau = 50$ fs [Eqs. (7) and (8)] throughout.

We use a laser pulse, defined by the electric-field vector

$$\mathbf{F}(t) = \mathbf{F}_0 \exp\left[-\left(\frac{t - MT_p/2}{MT_p/6}\right)^2\right] \sin\left(\frac{2\pi}{T_p}t\right)$$
$$\text{for } t \in [0, MT_p], \tag{45}$$

where $F_0 = |\mathbf{F}_0|$ is the peak electric-field strength, $T_p = 2\pi/\omega$ is the period of the field, with ω the driving frequency, and M is the number of cycles. We express the peak field strength in atomic units (a.u.)—1 a.u. of field strength is 5.142×10^{11} V/m.

The laser pulse used in the calculations of the harmonic yield in h-BN has a large but finite duration ($M = 48$ cycles) as opposed to the infinite periodic laser pulse used in the analysis in Sec. III. We have checked, however, that the position of the peaks is independent of the pulse duration (see the Appendix), so in the analysis below we assume that we are dealing with an infinite periodic field. Hence we will compare the numerical results solving the equations of motion (7) and (8) and using the field (45) with the analytical findings of Sec. III.

We consider the geometry where the field is oriented along the x axis [see Fig. 2]. Due to the breakdown of the inversion symmetry of h-BN with respect to the plane perpendicular to the electric field [Fig. 2(a)], even harmonics appear in the HHG spectrum. Here we concentrate on the intensity behavior of the first two harmonics in the HHG spectrum.

The first and the second harmonics of h-BN, obtained at different field strengths, are shown in Fig. 4. At small field strengths the shape of these responses is essentially perturbative, see Fig. 3 in Ref. [34] for the shape of the second harmonic in the perturbative limit. The perturbative first harmonic contains peaks for photon energies corresponding to the gap $\Delta = 7.8$ eV and to the Van Hove singularity [36] [the point where $\nabla_{\mathbf{k}} E_{c/v}(\mathbf{k}) = 0$, denoted as the M point in Fig. 2(b)] at a photon energy of $2[(\Delta/2)^2 + \gamma^2]^{1/2} \approx 9.09$ eV ($|f(\mathbf{k})| = 1$ at the Van Hove singularity). Peaks at these photon energies are visible also in the second-harmonic curves corresponding to the few lowest peak field strengths depicted in Fig. 4(b). In addition to these peaks, the second-order harmonic contains peaks at half of these frequencies [Fig. 4(b)], as it should [34].

Upon increasing the field strength, several features become apparent. First, peaks at photon energies, lower than the energies of the peaks in the perturbative responses, appear both in the first and in the second harmonic. Specifically, for the first harmonic, for $F_0 \geqslant 0.028$ a.u., broad peaks at $\sim$3.9 eV appear [Fig. 4(a)], while in the second harmonic, for $F_0 \geqslant 0.012$ a.u., peaks at $\sim$2.7 eV appear [Fig. 4(b)]. Second, some of the existing peaks, most notable example being the peak in the second harmonic corresponding to half of the gap [Fig. 4(b)], move as the peak field increases. This is also valid for the newly emerging peaks, which also move as the peak field increases [Fig. 4]. Finally, as the peak field increases, the peaks corresponding to the gap and the Van Hove singularity in the first harmonic decrease in height which can be seen from the curves corresponding to the first few peak fields [Fig. 4(a)]. The peak in the first harmonic at approximately 9.09 eV is due to the Van Hove singularity and occurs at the saddle point of the energy landscape. This peak is not due to the peak in the dipole matrix elements, but due to the peak in the density of states. As such it cannot be treated using the present approach. The same is true for the peak in the second harmonic, related to the Van Hove singularity (peak at 4.5 eV). In view of this, we apply the Floquet analysis only to the peaks corresponding and related to the gap, where the dipole matrix element peaks, and analyze the trends in the numerical data by using the theory developed in Sec. III.

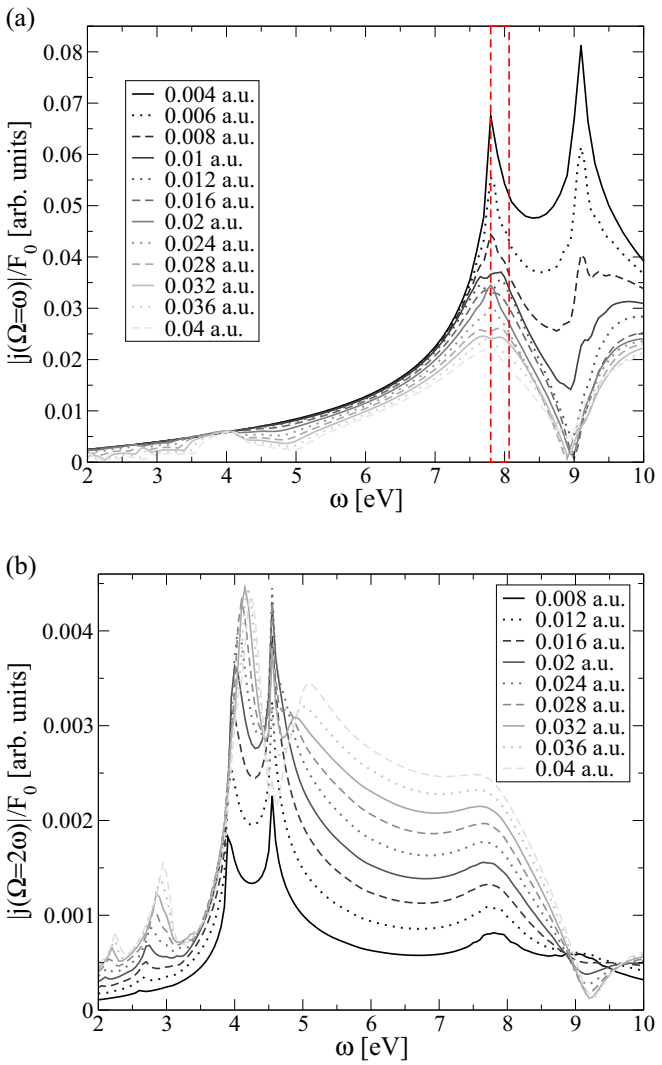

FIG. 4. (a) First and (b) second harmonic of h-BN for large field strengths, extracted from harmonic spectra induced by a 48-cycle pulse. The harmonic yield in panel (a) is proportional to $|\mathbf{j}(\Omega = \omega)|/F_0$, and the harmonic yield in panel (b) is proportional to $|\mathbf{j}(\Omega = 2\omega)|/F_0$. The peak field strengths F_0 at which different curves are obtained in panels (a) and (b) are given in the insets in atomic units. In panel (a), the dashed rectangle illustrates the extend of the peak shifting predicted by Eq. (37) (see text).

First, the bands are dressed by the field, so replicas of the conduction and valence bands appear, i.e., FB states, spaced by a photon energy, see the dashed lines in Fig. 3, sketched for the case $\hbar\omega = \Delta/2$. As the peak field strength increases, the FB shifts become evident in the first and the second harmonic in Fig. 4. For h-BN, the energy shifts of Eqs. (23) and (24)

calculated at the K point are

$$\Delta E_{c/v}|_{K\text{point}} = \pm\frac{3a^2\gamma^2}{8\Delta}\frac{e^2}{\hbar^2}\frac{F_0^2}{\omega^2} = \pm\Delta E. \quad (46)$$

In the above equation, "+" corresponds to ΔE_c, whereas "−" corresponds to ΔE_v. The total FB shift of the valence and conduction band is $E^{FB}(F_0,\omega) = 2\Delta E$. The ratio between the Bloch-Siegert shift and FB shift is explicitly $\hbar\omega/4\Delta$. Therefore, for the frequencies of interest, $\hbar\omega \leqslant \Delta$, the FB shift is clearly dominant.

To illustrate the manifestation of the FB shift in the harmonic spectra, we first consider the peak in the first harmonic at a photon energy corresponding to the gap at 7.8 eV. As evident from Fig. 4(a), the height of the peak decreases as the peak field strength increases. At larger field strengths the decrease of the peak is not as rapid, it seems that the peaks are not shifting, and even double peaks appear and disappear at some field strengths. A resonance frequency ω_R can be found that satisfies Eq. (37). The extent of the shifting predicted by Eq. (37) is illustrated in Fig. 4(a) by the dashed (red) rectangle, whose left side is at 7.8 eV (corresponding to the gap) and the right side of the rectangle is at 8.065 eV, which is exactly the gap plus the shift according to Eq. (37) at the largest field strength of 0.04 a.u. used. However, due to the direct (strong) coupling of strength $D/2$ between $(c,-1)$ and $(v,0)$ or, equally, between the states $(c,0)$ and $(v,1)$, the avoided crossing between these pairs of states widens at large field strengths. This is illustrated in Fig. 5 where the difference is shown between Floquet energies at the K point obtained by diagonalizing the Floquet matrix (34), with $\Delta D = 0$ and by using states (m,j) with $m = c,v$ and $j = -1,0,1$. In Fig. 5(a) resonant transition corresponds to a vanishing difference in energy of the states involved. From the figure it is clear that such a resonant frequency cannot be found for large field strengths. Therefore the height of the peak in the first harmonic at the gap decreases as the peak field increases [Fig. 4(a)].

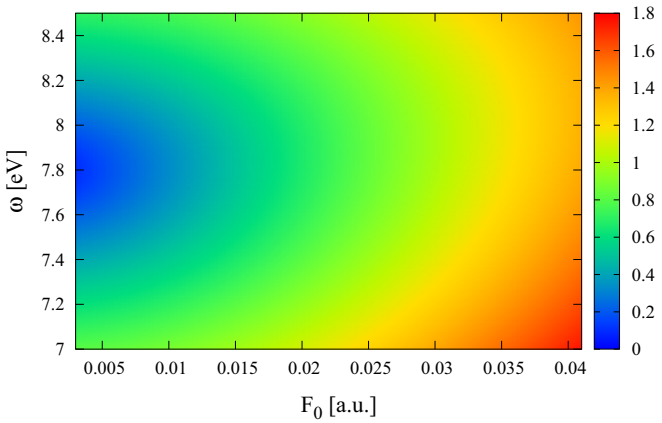

FIG. 5. The difference between the energies of the states $(c,-1)$ and $(v,0)$ or, equally the states $(c,0)$ and $(v,1)$ at the gap (K point), obtained by diagonalizing the Floquet matrix (34), with $\Delta D = 0$ and using states (m,j) with $m = c,v$ and $j = -1,0,1$ in the two dimensional space spanned by the field strength and the photon energy. The difference is measured in eV and color-coded on a linear scale.

The Rabi frequency $(D/\hbar)$ is taken into account in the explicit diagonalization to arrive at the result presented in Fig. 5. Also, the Rabi frequency is taken into account perturbatively in Eq. (37), expressed by the appearance of Bloch-Siegert shifts in that equation. At the highest field strength used, $F_0 = 0.04$ a.u., the inverse of the Rabi frequency is 3.12 fs, which is smaller than the decoherence time $\tau = 50$ fs. However, the inverse of the Rabi frequency is smaller than the total pulse duration at 7.8 eV, so full Rabi oscillations can occur within the pulse duration, which might be the reason behind the appearance of double peaks at certain field strengths.

To investigate the reason behind the peculiar behavior of the one-photon peaks, we have carried out numerical calculations restricted to a small area in $\mathbf{k}$ space around the K point, rather than including the whole Brillouin zone. In the limit of only taking the K point itself (two-level-system limit), we find that, for small field strengths ($F_0 < 0.004$ a.u.), the one-photon peak shifts according to the Bloch-Siegert shifts of Eq. (37), as it should. As more points in the vicinity of the K point are included, our calculations show that these $\mathbf{k}$ points coherently contribute to the one-photon peak. Therefore, the assumption that the shifting of the one-photon resonance can be described by using the properties of the two-band system at the gap only, one of the assumptions behind the derivation of Eq. (37), is not justified for the case of h-BN at the one-photon resonance. At photon energies not corresponding to the gap of h-BN, such an assumption is justified, as we will see from the numerical evidence below. We note that, in all cases, no matter how large a set of points around the K point is taken into account in the calculation, the resonance is rapidly lost as the field strength increases.

Next, we consider the field dependence of the peaks in the second harmonic corresponding to the gap, i.e., we consider the two-photon transition between the valence and conduction band, peaking around 3.9 eV for small field strengths; see Fig. 4(b). To recover the dependency of this peak on F_0 we calculate ω_R from Eq. (38). The position of peaks obtained this way agrees nicely with the peak positions extracted from the numerical calculation; see Fig. 6(a). With the increase of F_0 the peak moves to larger photon energy. This trend and also the values for the peaks is nicely described by using the FB shifts, especially at not-too-large photon energies.

Finally, we turn to the peaks in the low-order response that appear only for larger field strengths and that are not present in the perturbative result [34]. The presence of these peaks is evidence that a harmonic response can be resonant at energies smaller than the energy given by the gap and is entirely due to the formation of FB states in strong fields. We consider the most prominent peaks of this type, i.e., the peaks corresponding to the one-photon transition, peaking at $\sim\Delta/2 = 3.9$ eV in Fig. 4(a), and two-photon transition, peaking at $\sim\Delta/3 = 2.6$ eV in Fig. 4(b). In the first case, the one-photon transition should be resonant with the transition between the FB states of type $(c,j-1) \leftrightarrow (v,j)$. Hence, to obtain the dependence of the peak position on F_0, we determine ω_R from Eq. (38) at the gap. Figure 6(b) illustrates that the agreement between the peaks calculated that way with the numerically obtained positions of the peak is fair, even though

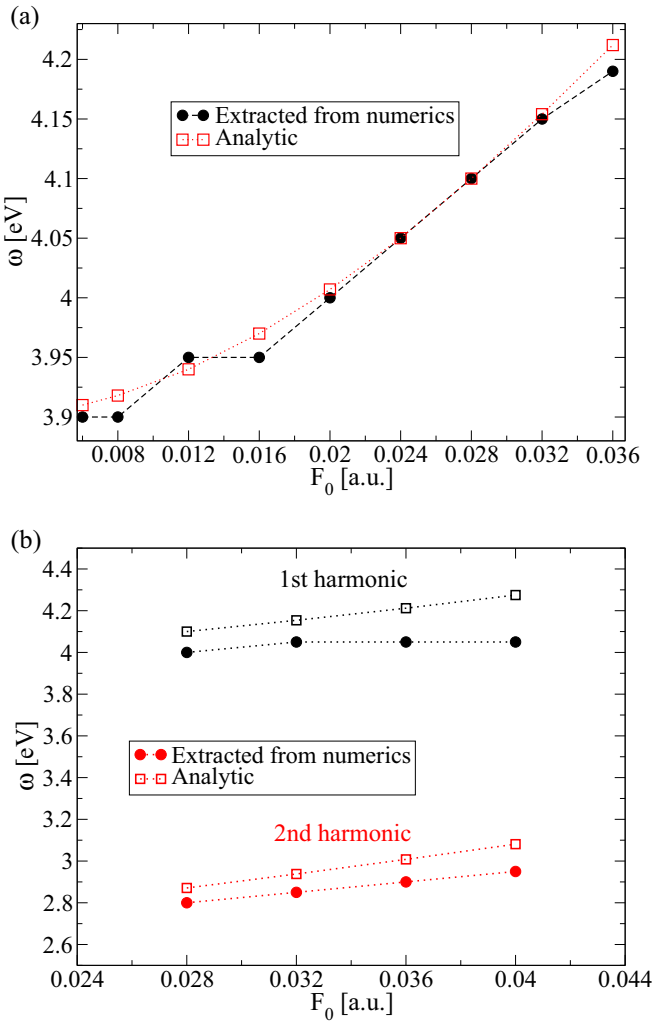

FIG. 6. Comparison of the peaks extracted from the numerical calculation for h-BN and the peaks corrected by including the Floquet-Bloch shifts, as a function of the peak field strength F_0 from Eqs. (38) and (47), respectively. (a) Peaks in the second harmonic corresponding to the transition at the gap. (b) Peaks corresponding to one-photon transition, peaking at $\sim\Delta/2$ in the first harmonic, and peaks corresponding to two-photon transition, peaking at $\sim\Delta/3$ in the second harmonic.

the theory slightly overestimates the shifts. The two-photon transition $(c, j-1) \leftrightarrow (v, j)$ peaking at $\sim\Delta/3$ is obtained as a crossing between (energy shifted) FB states $(c, j-3)$ and (v, j), i.e., from the equation

$$3\hbar\omega_R = \Delta + E^{FB}(F_0, \omega_R). \tag{47}$$

In Fig. 6(b) the frequency obtained from this approximation is compared with the position of the peaks extracted from the numerical calculation. The agreement is good.

V. CONCLUSIONS

The resonant peaks in the harmonic spectra as a function of the photon energy, present in the perturbative responses, shift due to the interaction with a strong laser pulse. Moreover, additional resonant peaks appear at energies corresponding to a fraction of the photon energy of the original peaks, which also shift as the laser pulse intensity changes. We find that appearance of new peaks is a signature of the formation of FB states. Another signature of the FB states specific to two-band systems is the field-dependent shifting of these peaks. We have investigated the dependence of the position of these peaks on the field strength and found a procedure to analyze it by making an analogy to the case of a two-level atom. The shifts of the peaks as a function of the field are mainly due to the FB shifts, introduced in this work, which are larger than the Bloch-Siegert shifts but of the same order in the peak field strength as the Bloch-Siegert shifts. We derived an analytic formula for the FB shift [Eq. (25)]. This analytic form was verified by comparison with explicit numerical calculations of the harmonic spectra for h-BN.

The FB shift, involving the reduced effective mass, is formally identical to the ponderomotive shift appearing in the strong-field physics of atoms and molecules. In a two-band system the shift is such that both valence and conduction band shift in a direction that leads to an increase of the gap as the laser intensity increases. On the basis of the analogy with the ponderomotive shift, a measure for the validity of the perturbative response was derived, expressed by the smallness of the ratio between the FB shift and the gap.

The FB shifts reported here should appear for any two-band semiconductor, and we also expect them to appear when semiconductors are treated by using multiple bands, and when excitons are included. The extent to which the shifts are visible in the spectrum will depend on the peaking of the dipole matrix element at the gap and its associated ability to produce visible, well-pronounced resonances in the harmonic response. The recent advances in strong-field physics in solids [37–40] create the possibility of an experimental investigation of the ideas discussed here.

ACKNOWLEDGMENTS

This work was supported by the Villum Kann Rasmussen (VKR) Center of Excellence QUSCOPE. The numerical results were obtained at the Centre for Scientific Computing, Aarhus.

APPENDIX

Here we show that the positions of the peaks that we analyze in the main text do not depend on the pulse duration by performing explicit numerical calculation and comparing the first and second harmonic for pulses of the type given in Eq. (45) for 24, 48, and 96 cycles. To compare the harmonic spectra directly between pulses with different finite duration, the spectra are scaled by dividing by the pulse duration MT_p; see also Eq. (15) and the discussion in the paragraph after Eq. (16) in Ref. [19]. In Fig. 7 we compare the first [Figs. 7(a) and 7(b)] and the second harmonic [Figs. 7(c) and 7(d)] at small $F_0 = 0.008$ a.u. [Figs. 7(a) and 7(c)], and at large field $F_0 = 0.032$ a.u. [Figs. 7(b) and 7(d)]. From the figure, it is clear that the positions of the peaks that we are able to analyze analytically (those that that are not due to the Van Hove singularity) are indeed unaffected by the pulse duration.

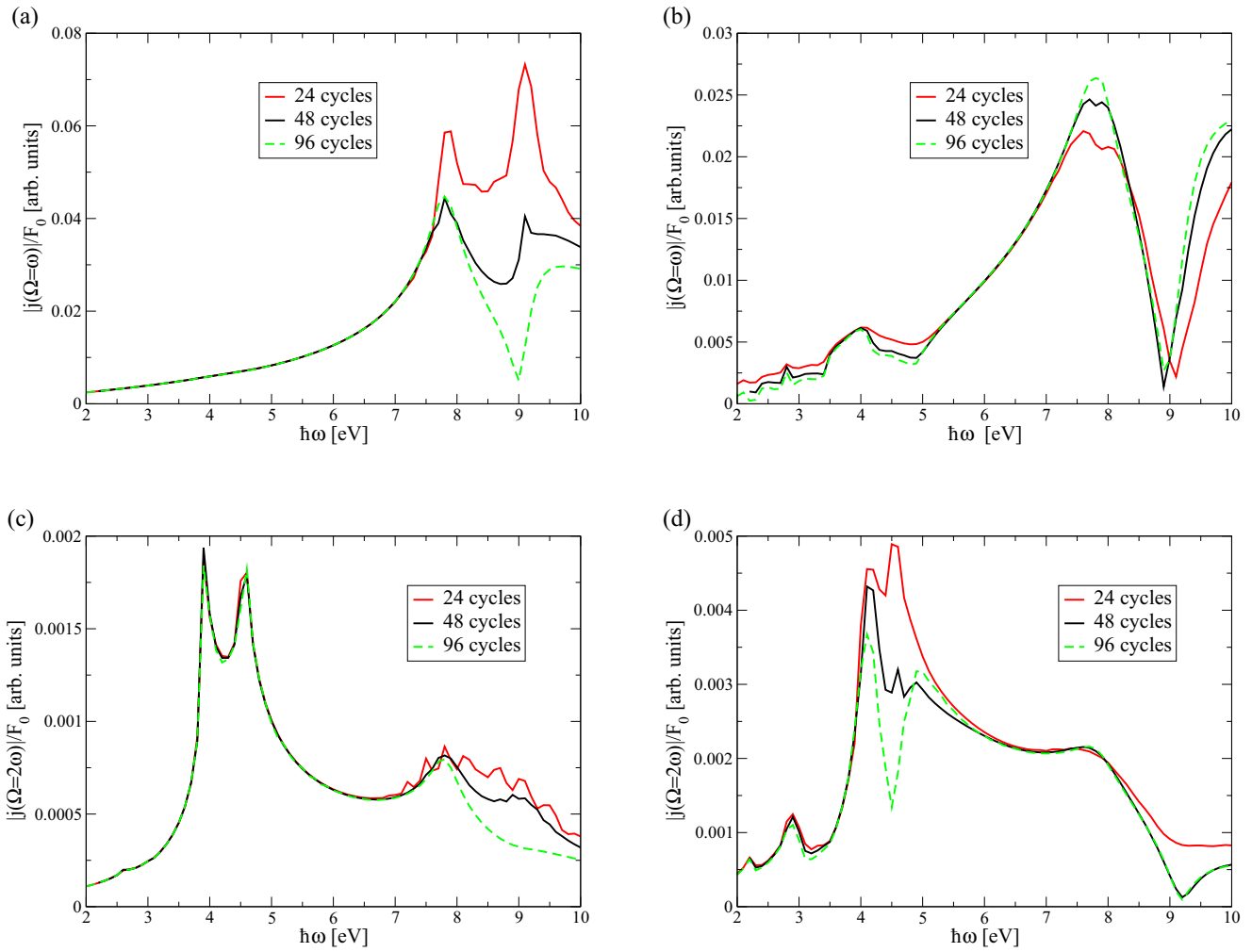

FIG. 7. The dependence of the first harmonic [panels (a) and (b)] and the second harmonic [panels (c) and (d)] on the number of field cycles, M; see Eq. (45). Panels (a) and (c) contain the harmonics at smaller field strength $F_0 = 0.008$ a.u., whereas the harmonics for $F_0 = 0.032$ a.u. are given in panels (b) and (d).

[1] J. H. Shirley, Phys. Rev. **138**, B979 (1965).

[2] N. W. Ashcroft and N. D. Mermin, *Solid State Physics*, International ed. (W. B. Saunders Company, Philadelphia, 1976).

[3] F. H. M. Faisal and J. Z. Kamiński, Phys. Rev. A **56**, 748 (1997).

[4] Y. H. Wang, H. Steinberg, P. Jarillo-Herrero, and N. Gedik, Science **342**, 453 (2013).

[5] F. Mahmood, C.-K. Chan, Z. Alpichshev, D. Gardner, Y. Lee, P. A. Lee, and N. Gedik, Nat. Phys. **12**, 306 (2016).

[6] H. Hsu and L. E. Reichl, Phys. Rev. B **74**, 115406 (2006).

[7] T. Oka and H. Aoki, Phys. Rev. B **79**, 081406 (2009).

[8] Y. Zhou and M. W. Wu, Phys. Rev. B **83**, 245436 (2011).

[9] S. T. Park, Phys. Rev. A **90**, 013420 (2014).

[10] S. Y. Zhou, G.-H. Gweon, A. V. Fedorov, P. N. First, W. A. de Heer, D.-H. Lee, F. Guinea, A. H. Castro Neto, and A. Lanzara, Nat. Mater. **6**, 770 (2007).

[11] E. V. Castro, K. S. Novoselov, S. V. Morozov, N. M. R. Peres, J. M. B. Lopes dos Santos, J. Nilsson, F. Guinea, A. K. Geim, and A. H. Castro Neto, Phys. Rev. Lett. **99**, 216802 (2007).

[12] X. Li, X. Wang, L. Zhang, S. Lee, and H. Dai, Science **319**, 1229 (2008).

[13] T. G. Pedersen, C. Flindt, J. Pedersen, N. A. Mortensen, A.-P. Jauho, and K. Pedersen, Phys. Rev. Lett. **100**, 136804 (2008).

[14] T. G. Pedersen, C. Flindt, J. Pedersen, A.-P. Jauho, N. A. Mortensen, and K. Pedersen, Phys. Rev. B **77**, 245431 (2008).

[15] V. A. Margulis, E. E. Muryumin, and E. A. Gaiduk, Phys. Rev. B **77**, 035425 (2008).

[16] K. F. Mak, C. Lee, J. Hone, J. Shan, and T. F. Heinz, Phys. Rev. Lett. **105**, 136805 (2010).

[17] H. Liu, Y. Li, Y. S. You, S. Ghimire, T. F. Heinz, and D. A. Reis, Nat Phys **13**, 262 (2016).

[18] C. Aversa and J. E. Sipe, Phys. Rev. B **52**, 14636 (1995).

[19] D. Dimitrovski, L. B. Madsen, and T. G. Pedersen, Phys. Rev. B **95**, 035405 (2017).

[20] J. B. Krieger and G. J. Iafrate, Phys. Rev. B **33**, 5494 (1986).

[21] J. B. Krieger and G. J. Iafrate, Phys. Rev. B **35**, 9644 (1987).

[22] G. Vampa, C. R. McDonald, G. Orlando, D. D. Klug, P. B. Corkum, and T. Brabec, Phys. Rev. Lett. **113**, 073901 (2014).

[23] L. Plaja and L. Roso-Franco, J. Opt. Soc. Am. B **9**, 2210 (1992).
[24] L. Plaja and L. Roso, J. Mod. Opt. **40**, 793 (1993).
[25] A. E. Kaplan and P. L. Shkolnikov, Phys. Rev. A **49**, 1275 (1994).
[26] A. Picón, L. Roso, J. Mompart, O. Varela, V. Ahufinger, R. Corbalán, and L. Plaja, Phys. Rev. A **81**, 033420 (2010).
[27] M. Wu, D. A. Browne, K. J. Schafer, and M. B. Gaarde, Phys. Rev. A **94**, 063403 (2016).
[28] G. Ndabashimiye, S. Ghimire, M. Wu, D. A. Browne, K. J. Schafer, M. B. Gaarde, and D. A. Reis, Nature (London) **534**, 520 (2016).
[29] F. Bloch and A. Siegert, Phys. Rev. **57**, 522 (1940).
[30] L. V. Keldysh, Zh. Eksp. Teor. Fiz. **47**, 1945 (1964) [Sov. Phys. JETP **20**, 1307 (1965)].
[31] H. Reiss, Prog. Quantum Electron. **16**, 1 (1992).
[32] P. R. Wallace, Phys. Rev. **71**, 622 (1947).
[33] T. G. Pedersen, A.-P. Jauho, and K. Pedersen, Phys. Rev. B **79**, 113406 (2009).
[34] T. G. Pedersen, Phys. Rev. B **92**, 235432 (2015).
[35] I. Al-Naib, J. E. Sipe, and M. M. Dignam, Phys. Rev. B **90**, 245423 (2014).
[36] L. Van Hove, Phys. Rev. **89**, 1189 (1953).
[37] S. Ghimire, A. D. DiChiara, E. Sistrunk, P. Agostini, and D. A. DiMauro, Louis F. Reis, Nat. Phys. **7**, 138 (2011).
[38] T. T. Luu, M. Garg, S. Y. Kruchinin, A. Moulet, M. T. Hassan, and E. Goulielmakis, Nature (London) **521**, 498 (2015).
[39] G. Vampa, T. J. Hammond, N. Thire, B. E. Schmidt, F. Legare, C. R. McDonald, T. Brabec, and P. B. Corkum, Nature (London) **522**, 462 (2015).
[40] M. Hohenleutner, F. Langer, O. Schubert, M. Knorr, U. Huttner, M. Koch, S. W. Kira, and R. Huber, Nature (London) **523**, 572 (2015).